Characterization of Nanostructure of Stimuli-Responsive Polymeric Composite Membranes

ARTICLE *in* BIOMACROMOLECULES · JULY 2004

Impact Factor: 5.75 · DOI: 10.1021/bm034458f · Source: PubMed

Characterization of Nanostructure of Stimuli-Responsive Polymeric Composite Membranes

Kai Zhang,[†,§] Huiyu Huang,[†] Guocheng Yang,[‡] James Shaw,[‡] Christopher Yip,[‡] and Xiao Yu Wu*[,†]

Faculty of Pharmacy and Institute of Biomaterials & Biomedical Engineering, University of Toronto, Toronto, Ontario, M5S 2S2 Canada

Received November 6, 2003; Revised Manuscript Received March 4, 2004

To elucidate the mechanism of stimuli-responsive permeability and to optimize the design, the nanostructure of polymeric composite membranes, developed in our laboratory, was characterized. The membranes were prepared to contain various amounts of stimuli-responsive nanoparticles of poly(*N*-isopropylacrylamide-*co*-methacrylic acid), with or without polyelectrolyte coating. Scanning electron microscopy and X-ray photoelectron spectroscopy were used respectively to examine the morphology and surface chemical composition, whereas atomic force microscopy and laser scanning confocal microscopy were employed to characterize the in situ surface and internal structure of the membranes in aqueous media of various pHs. The porous structure was evidenced in the presence of the nanoparticles. The surface content of the nanoparticles increased with increasing particle concentration while the polyelectrolyte coating was nearly undetectable. AFM images revealed that the particles in the membranes shrank with a concomitant increase in pore size as the buffer pH decreased. LSCM results indicated that particles were distributed through the membrane as interconnected clusters.

Introduction

Drug delivery systems with temperature- or pH-sensitivity have drawn much attention due to their ability to regulate drug release in response to internal or external stimuli.[1−3] Various systems have been designed with utilization of different structures and mechanisms including stimulus-dependent swelling of hydrogels.[1−10] These hydrogels have been used as bulk matrixes, as membranes, or as controlling valves in a device or in a composite membrane. A polymeric composite membrane system responsive to changes in temperature and pH was previously developed in our laboratory by dispersing poly(*N*-isopropylacrylamide-*co*-methacrylic acid) (poly(NIPAAm-*co*-MAA)) nanoparticles in an ethylcellulose matrix.[9−14] In such a membrane, while the inert ethylcellulose matrix offers good mechanical strength, the hydrogel nanoparticles, with $T_{tr} \sim 37$ °C and p$K_a \sim 5.5$, undergo swelling-shrinking cycles with changes in temperature or pH,[14−17] imparting stimulus-sensitive permeability to the system. Previous studies have shown that solute permeability across the composite membranes is higher at elevated temperature or glucose concentration or at lower pH.[9−14]

The influence of nanoparticle composition and concentration in the membrane has been investigated using solutes of various molecular sizes such as acetaminophen (MW 151, R_h 2.4 Å), vitamin B12 (1355, R_h 8.5 Å), insulin (MW ∼6,000 and R_h 10 × 16 Å).[10−14] It has been found that, as the molar ratio of NIPAAm to MAA increases from 1:0.1 to 1:1, the solute permeability of the membranes is changed from more thermal responsive to more pH sensitive. In other words, the membranes containing nanoparticles with higher NIPAAm content exhibit higher thermal responsiveness, whereas those with higher MAA content demonstrate higher pH sensitivity.[11−14] The temperature or pH induced permeability changes have been found to be greater for the solutes with molecular weights ranging from one thousand to a few thousands than those for the small molecules such as acetaminophen. However, proteins with molecular weights of over 10 000 like lysozyme (MW 14,400 and R_h 20.5 Å) have difficulty in permeating the membrane under all studied conditions, suggesting that the membranes have the potential to protect enclosed enzyme-labile compounds from degradation.

The membrane permeability increases drastically as the nanoparticle concentration is raised to 30 wt % or higher, implying that the particle concentration reaches a percolation threshold.[14] The morphological study of the membranes containing 0, 19, 30, 40, or 50 wt % of the nanoparticles using scanning electron microscopy (SEM) has revealed that the porosity of the membranes at dry state depends on the particle content.[14] Considering a low mechanical strength of the membranes with 40 wt % or more nanoparticles and a low permeability of the membranes with less than 20% of the nanoparticles, the membranes containing 30−35 wt % of the nanoparticles have been selected for further investigations.[13,14,18]

* To whom correspondence should be addressed. Phone: +1 416-978-5272. Fax: +1 416-978-8511. E-mail: xywu@phm.utoronto.ca.

[†] Faculty of Pharmacy.

[‡] Institute of Biomaterials & Biomedical Engineering.

[§] Current address: Patheon Inc., 2100 Syntex Court, Mississauga, ON, L5N 7K9 Canada.

10.1021/bm034458f CCC: $27.50
Published on Web 04/15/2004

On the basis of these findings and the temperature- and pH-responsive behavior of the nanoparticles, we have proposed that solutes mainly diffuse through the channels formed by connected particles when the particle concentration in a membrane is higher than 20−30 wt %.[11−14] The solutes can permeate through the membrane via both intraparticulate pathway and interparticulate pathway. At $T < T_{tr}$ or pH > pK_a, the particles are highly swollen occupying most of the pore space. Thus, the solutes mainly diffuse through the gel phase of the swollen nanoparticles. At $T > T_{tr}$ or pH < pK_a, the particles collapse generating large, water-filled pores that become a major pathway for solute diffusion. Thereby, the positive temperature sensitivity and negative pH sensitivity of the membranes have been obtained.[11−14]

However, up to date, no direct evidence has been collected in situ showing particle-shrinking-swelling and consequent pore-enlarging-closing in the membranes at a wet state. For this reason, a special experiment was designed in this work to visualize the change of particle volume and pore size with pH in buffer solutions with atomic force microscopy (AFM). In this case, the most pH-sensitive membrane, among all investigated before, was used, consisting of 35 wt % of the nanoparticles with 1:1 molar ratio of NIPAAm to MAA. Owing to a similarity between swelling-shrinking of the particles in response to pH and to temperature changes, it was hoped that the result of AFM imaging at various pHs could be extended to explain the thermoresponsive structural change of the membranes.

During the course of this work and previous studies, leakage of the nanoparticles on the membrane surface was sometimes observed. Hence, coating of the membranes with polyeletrolyte layers was attempted to improve the quality of the membranes. The effect of the coating on the nanostructure of the membrane and its in situ pH sensitivity was examined by AFM. The surface chemical composition of the membranes was measured by X-ray photoelectron spectroscopy and the surface and internal structure of the membranes in buffer solutions was determined by laser scanning confocal microscopy.

Materials and Methods

Materials. Methacrylic acid (MAA, Aldrich) was made inhibitor free by distillation. *N*-Isopropylacrylamide (NIPAAm, Eastman Kodak) was purified by recrystallization from hexane and toluene. *N*,*N*′-Methylenebisacrylamide (BIS, Aldrich), sodium dodecyl sulfate (SDS, Mallinckrodt), potassium persulfate (KPS, Aldrich) and ethylcellulose (viscosity 45, Dow Chemical Company) were used as received. Fluoresceinamine isomer I (FA), 1-ethyl-3-(3-dimethylaminopropyl)-carbodiimide hydrochloride (EDCH), poly(acrylic acid) (PAA, M_w 90 000), and poly(allylamine hydrochloride) (PAH, M_w 70 000) were purchased from Aldrich Chemical Co., and used without further treatment.

Membrane Preparation. *(1) Synthesis and Characterization of Poly(NIPAAm-co-MAA) nanoparticles.* Temperature-/pH-responsive nanoparticles of NIPAAm and MAA with a molar ratios 1:1 were synthesized by aqueous dispersion polymerization.[16] NIPAAm, MAA, and BIS were mixed in a molar ratio of 1:1:0.068 to total 135 mM in concentration. 0.4 mM SDS was used to stabilize the system. The mixture was first heated to 70 °C and purged with N_2, then 2.1 mM KPS was added to initiate the polymerization. The reaction was carried out at 70 °C under a N_2 blanket for 4 h with constant stirring at 200 rpm. The nanoparticles with a yield of over 99% were then purified by membrane dialysis against distilled deionized (DDI) water using Spectra/Pro (Fisher Scientific) with a molecular weight cutoff of 12 000−14 000. Particle size and size distribution of the resultant nanoparticles at room temperature and at 37 °C in DDI water and in phosphate buffer solutions of various pH (pH 5, 6, and 7.4, 0.15 M) were measured on a dynamic laser scattering (DLS) particle sizer (NICOMP, Model 380 ZLS).

(2) Preparation of Fluoresceinamine-Labeled Nanoparticles. To study the distribution of the nanoparticles in the composite membranes, the particles were labeled with fluoresceinamine using a method by Horisawa et al.[19] prior to their incorporation into the membranes. A suspension was prepared by dissolving 0.0439 g of FA and 0.0316 g of EDCH into 30 mL of dimethyl sulfoxide (DMSO), followed by addition of 0.50 g of poly(NIPAAm-*co*-MAA) nanoparticles. The suspension was then incubated at room temperature for 20 h. The resultant fluoresceinamine bound nanoparticles were washed with DDI water several times, centrifuged, and dried at room temperature in a vacuum oven (Vacuum Oven 280, Fisher Scientific). Particle size and size distribution in DDI water at ambient temperature were measured using the dynamic laser scattering particle sizer and compared with particles without the labeling.

(3) Preparation of Temperature-/pH-Responsive Membranes. A solution casting method was employed to prepare the membranes.[11−14] In this process, the purified nanoparticles were dried, dispersed in 100% ethanol, and then added to an ethanol solution of ethylcellulose with desirable contents. After being mixed thoroughly, the mixture was poured into a glass dish and kept in a desiccator. The membranes formed after evaporation of the solvent were then cleaned and stored in DDI water at room temperature. The actual membrane thickness was measured with a micrometer (Fowler, Inc.).

(4) Membrane Surface Coating with Polyelectrolytes. A composite membrane with 35 wt % of 1:1 nanoparticles was coated with multilayers of polyelectrolytes by alternating deposition of PAH and PAA following a method described in the literature.[20,21] The concentration of aqueous solutions of the polyeletrolytes was 0.01 M, and the pH of the solutions was adjusted to pH 6.5 using 0.1 M NaOH or HCl. The membrane was first immersed in PAH for 15 min and rinsed in DDI water three times (3 min each time). It was then immersed in PAA for 15 min, followed by the same rinse procedure. The process was repeated three cycles resulting in tri-layerpairs on the membrane.

Membrane Characterization. SEM was employed to study the membrane structure in the dry state, whereas AFM and LSCM were used to investigate in situ membrane structure. XPS served as a tool for analyzing chemical composition of membrane surface.

(1) Scanning Electron Microscopy (SEM). SEM photographs were obtained using a Hitachi-2500 microscope at

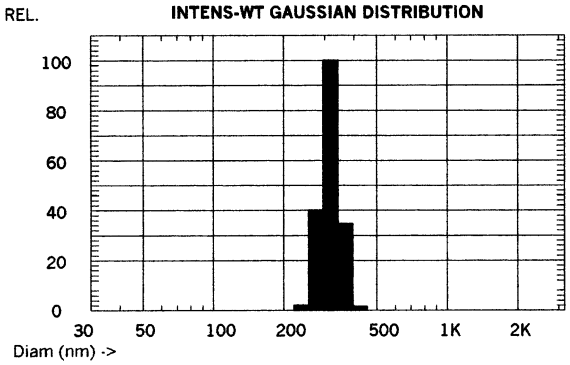

Figure 1. Intensity-weighted gaussian distribution of diameters of poly(NIPAAm-*co*-MAA) nanoparticles in pH 5 PBS at 37 °C.

20 kV. The top and bottom surfaces and cross-section area of a membrane were studied. For the cross-section area study, membrane samples were freeze-dried, fractured mechanically, and fixed onto the sample holders with a double-sided tape. For the surface area study, air-dried membranes were directly fixed onto the sample holders with the double-sided tape. All of the samples were vapor coated with gold in a sputter coating system before being scanned.

(2) X-ray Photoelectron Spectroscopy (XPS). XPS spectra were obtained on a Leybold MAX 200 XPS system (LH, Cologne, Germany) using an unmonochromatized Mg Kα source operating at 15 kV and 20 mA. The energy scale was corrected by placing the C 1s value for the main C−C component at 285 eV. Atomic ratios were obtained from spectra collected in a low-resolution mode, whereas other chemical information was obtained from high-resolution spectra. A spectrum fitting was performed using Spec Lab (Surface/Interface Inc., Mountain View, CA).

(3) Atomic Force Microscopy (AFM). Solution tapping mode atomic force microscopy (TMAFM) images were acquired on a Digital Instruments Nanoscope IIIA Multimode scanning probe microscope (Digital Instruments, Santa Barbara, CA) using 120 μm oxide-sharpened silicon nitride V-shaped cantilevers installed in a combination contact/tapping mode liquid flow cell. The flow cell was fitted with inlet and outlet tubes to enable direct fluid exchange during imaging. A membrane was mounted onto a piece of freshly cleaved mica, sealed in the flow through cell, and allowed to soak in the solution for 30 min to reach swelling equilibrium before the height and phase images were acquired. The AFM cantilevers were irradiated with UV light prior to imaging to remove any adventitious organic contaminations. The AFM images were acquired using the E scanning head, which has a maximum lateral scan area of

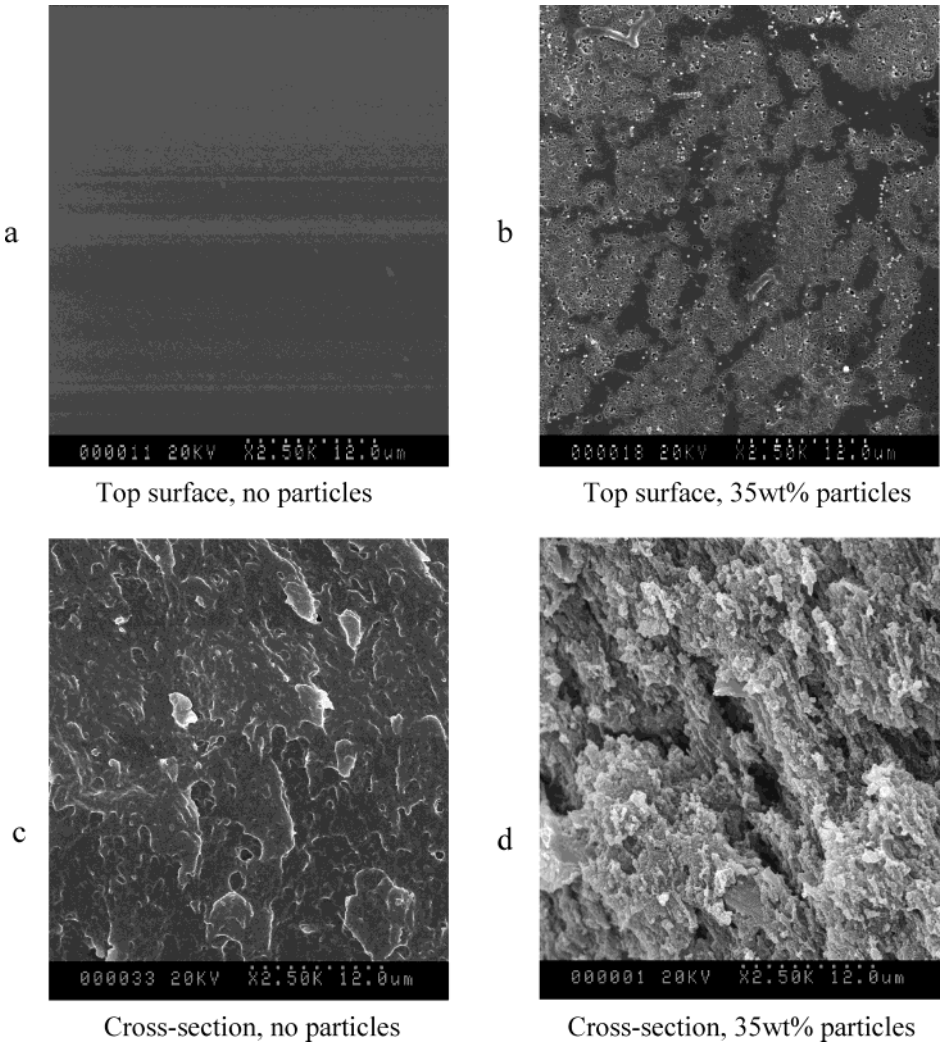

Figure 2. SEM photographs of top surfaces of membranes with 0% (a) or 35 wt % particles (b) and cross-sections of membranes with 0% (c) or 35 wt % particles (d).

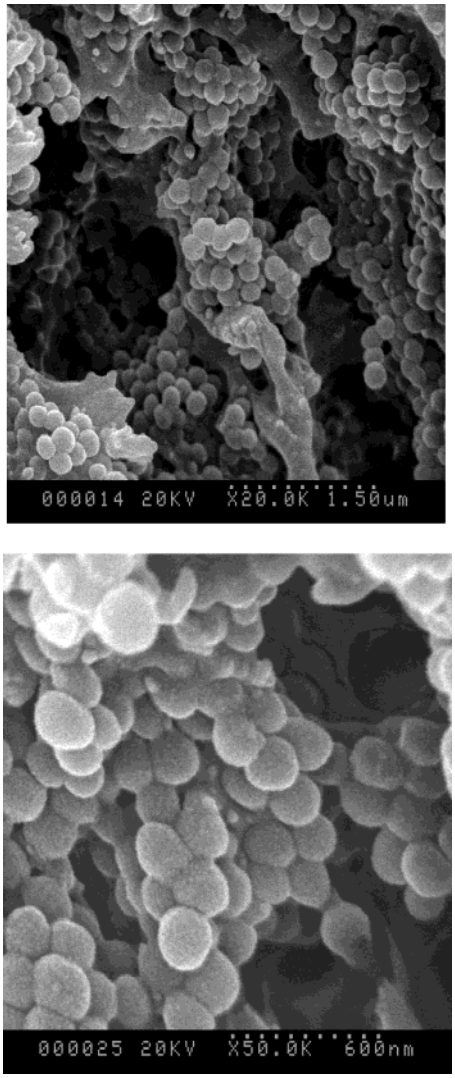

Figure 3. SEM photographs of cross-section of a membrane with 35 wt % of particles.

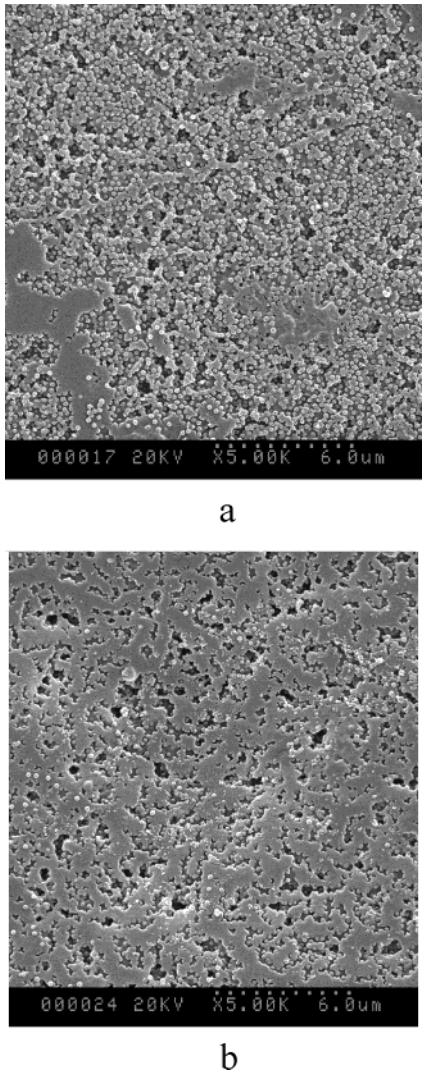

Figure 4. SEM photographs of top (a) and bottom (b) surface for a membrane with 35 wt % of particles.

$14.6 \times 14.6\ \mu$m. All imaging was performed at tip scan rates from 1 to 0.5 Hz, using cantilever drive frequencies of ~8.9 kHz at ambient temperature. All images were captured as 512×512 pixel images. Feature size and volume were calculated using the Digital Instruments Nanoscope software (version 4.21) and a shareware image analysis program, NIH image (version 1.62).

(4) Laser Scanning Confocal Microscopy (LSCM). The in situ internal membrane structure was investigated using a fully automatic Fluoview 500 and a Fluoview 300 laser scanning confocal microscope (Olympus, Japan) equipped with blue Ar (488 nm), green He Ne (543 nm), as well as red He Ne (633 nm) lasers at ambient temperature. While simultaneously acquiring the optical sections of the fluorescence emission from the fluoresceinamine-labeled nanoparticles using the argon laser as well as the overall laser backscattering properties of the composite membrane using the red He Ne laser, the membrane was immobilized in an Attofluor imaging chamber (Molecular Probes Inc.) and immersed in DDI water. A 510−530 nm band-pass filter and a 605 nm long-pass filter were used respectively to collect appropriate fluorescence and scattering signals. The data were analyzed with Fluoview software and Image Pro Plus (version 4.5).

Results and Discussion

1. Particle Size and Size Distribution. Figure 1 illustrates a typical plot of particle size distribution determined by the DLS method. For the nanoparticles studied in the work, the mean diameter ± the standard deviation at 37 °C was obtained to be 318.2 ± 32.5 nm (pH 5), 439.2 ± 60.2 nm (pH 6), and 477.3 ± 104.5 nm (pH 7.4). After fluorescence labeling, the nanoparticles did not show a noticeable change in particle size with a mean diameter around 500 nm in DDI water at ambient temperature. The size and morphology of the particles at dry state can also be visualized in the SEM photographs presented later.

2. Membrane Structure in a Dry State. The surface and cross section of a pure ethylcellulose membrane and a membrane with 35 wt % of 1:1 nanoparticles were characterized using SEM. Their microscopic photographs are presented in Figures 2−4. A great difference in morphology is evidenced by Figure 2 between the membrane with and without the nanoparticles. The ethylcellulose membrane is

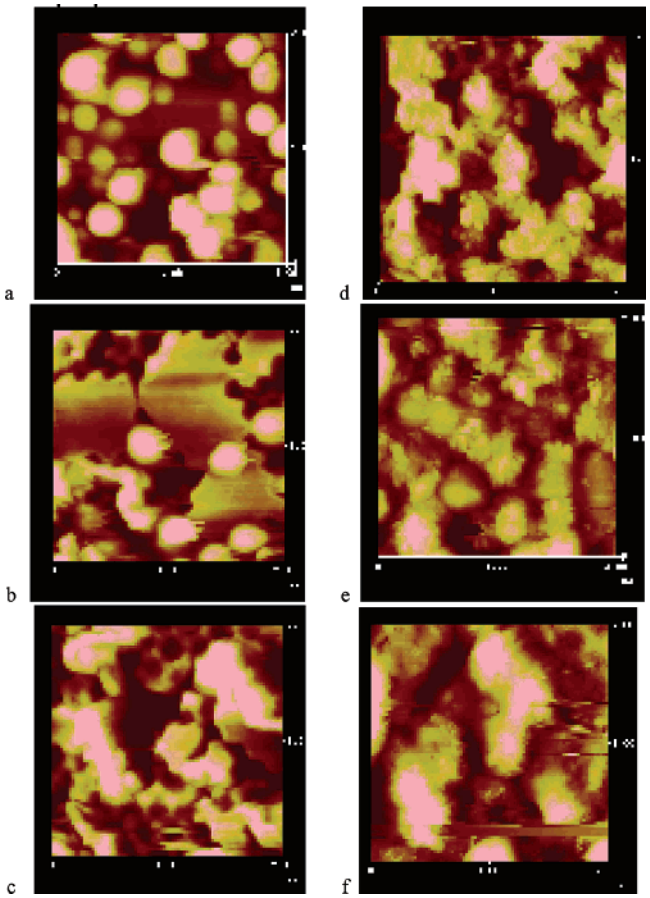

Figure 5. Topographical images of membranes containing 35 wt % of nanoparticles with (d−f) or without coating of polyelectrolytes (a−c). The membranes were immersed in a PBS buffer of pH 5 (a and d), then pH 6 (b and e), and finally pH 7.4 (c and f) at room temperature. Image size: 2 μm × 2 μm.

dense with virtually no pores (Figure 2, parts a and c), whereas the composite membrane has a spongelike internal structure and porous surface (Figure 2, parts b and d). Such a porous structure can be credited to the presence of the nanoparticles in the membrane which is a causal factor of stimuli-responsive permeability of the membrane. Our previous study has demonstrated that the membrane porosity and the pore size increase with increasing particle concentration in the membrane.[14]

Further examination using a higher magnification (Figure 3) reveals that the ethylcellulose constitutes the frame of the pores that are formed by collapsed, dried nanoparticles. Conceivably, these nanoparticles occupy the pore space when they are swollen in a medium, which is demonstrated by in situ examination using AFM (see next section). Because of the difference in hydrophilicity between ethylcellulose and the nanoparticles, the particles tend to aggregate forming clusters resulting in uneven distribution in the membrane. As the particle concentration increases, the aggregates become bigger, and thereby larger pores and higher porosity are produced upon particle collapse.[14]

Figure 4 presents SEM photographs of top (a) and bottom (b) surfaces of a membrane. The former is the surface in contact with air and the latter in contact with the glass dish during the fabrication process. It shows that more particles stay on the top surface than on the bottom, which may be

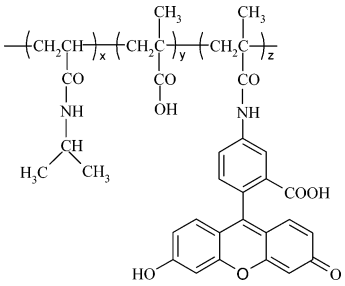

Figure 6. Chemical structure of fluoresceinamine used to label the nanoparticles.

caused by the density difference between the swollen particles and the ethylcellulose solution during membrane fabrication process.

3. Surface Structure of the Membranes in Phosphate Buffer Solutions (PBS) of Varied pH Values. The membranes containing 35 wt % of 1:1 nanoparticles were immersed in 0.15 M PBS solutions of pH 5, 6, or 7.4 at ambient temperature and examined in situ using AFM. The topographical images of the membrane without polyeletrolyte coating (left) and with coating (right) are shown in Figure 5, where the light spots represent nanoparticles on the surface and the dark regions indicate pores and deeper areas. It is seen that the light spots are smaller and more isolated at lower pH (e.g., pH 5). Meanwhile, the dark regions shrink as the pH increases. This result is consistent with the pH-dependent swelling of the nanoparticles. As reported previously, the particle size increases with increasing pH owing to more ionization of MAA units.[15,16] This direct visualization of pH-dependent change in pore size supports the proposed mechanism of pH-responsive delivery of drugs through these types of composite membranes.[11,12,14] Though the AFM imaging was not conducted at various temperatures, it is conceivable that the similar mechanism is applicable to thermoresponsive permeability of the membranes because the particles shrink at higher temperatures[15−17] resulting in a larger pore size in the membrane.

It is noticed from the AFM pictures that, without the surface coating with the polyelectrolytes, some nanoparticles on the surface escaped from the membrane at higher pH during imaging, leaving holes with the shape of the particles (Figure 5a−c). This phenomenon is likely due to a reduction in the adhesive forces (e.g., van der Waals force and hydrogen bonding) binding the particles to the membrane matrix at higher pH. When the particles become more hydrophilic, they are less miscible with the hydrophobic ethylcellulose. In the meantime, the particles become larger as the ionization degree increases, which may also cause the particles to pop out from the surface. Besides, slight friction between the AFM probe and the particles in the process scanning could facilitate the particle detaching from the membrane. Note that particles inside the membrane should remain bound because of the physical hindrance from the membrane framework.

To prevent particle loss from the surface of the membrane, tri-layerpairs of PAA and PAH were coated onto the membrane. Figures 5d−f illustrate that the holes of particle shape are dramatically diminished indicating that escape of the particles is significantly reduced with the coating. On

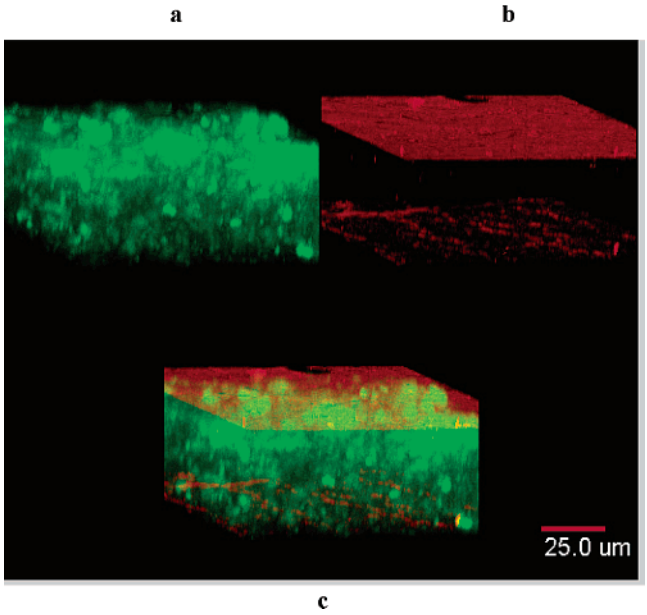

Figure 7. 3D Reconstruction of a composite membrane with 35 wt % 1:1 nanoparticles immersed in DDI water at room temperature with (a) distribution of fluoreceinamine-labeled nanoparticles in the composite membrane, (b) laser light backscattering properties of the composite membrane, and (c) superimposition of (a) and (b). Image size: 2 μm $\times$ 2 μm.

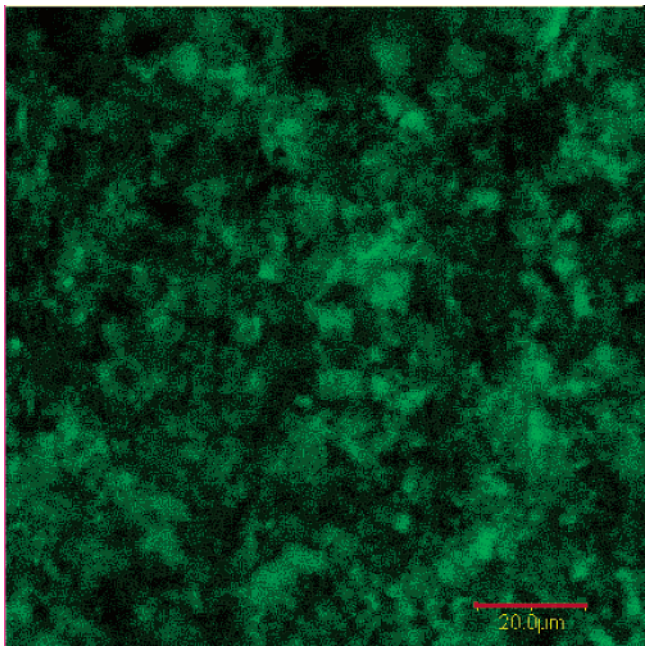

Figure 8. Fluorescence optical section of a membrane halfway from membrane surface. The membrane with 35 wt % of 1:1 nanoparticles was immersed in DDI water at room temperature.

the other hand, the particle shape is less spherical attributable to the presence of the polyelectrolyte network and its interaction with the particles. Whether this interaction would affect the stimuli-responsive permeability of the membrane is being investigated in our laboratory.

4. Particle Distribution in a Membrane. The internal structure of a membrane with 35 wt % of fluoresceinamine-modifiedparticles was studied in situ using LSCM in DDI water at ambient temperature. It is assumed that the distribution of the fluorescence labeled particles in the membrane is representative of that of the unmodified particles because

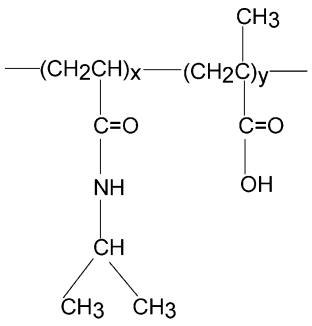

Poly(NIPAAm-co-MAA)

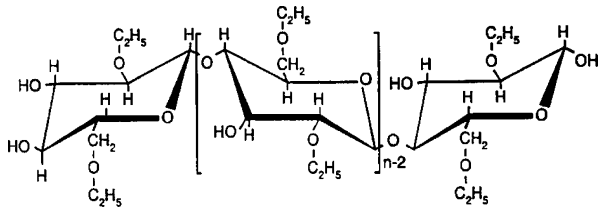

Ethylcellulose

Figure 9. Chemical structures of nanoparticles and ethylcellulose.

Table 1. Elemental Analysis of Membranes by XPS

	relative abundance (wt % of nanoparticles in the membrane)		
element	0	19	35
C	69.1	70.7	70.4
N	0	3.0	5.8
O	30.9	25.9	23.0

Table 2. Carbon 1s Envelope Analysis of Membranes

	relative abundance (wt % of nanoparticles in the membrane)		
carbon type	0	19	35
C−C/C−H	36.6	38.6	43.7
C−O/C−N	48.5	39.4	31.7
O−C−O	10.5	16.9	19.3
O−C=O	4.4	5.1	5.3

of a low concentration and hydrophilicity of fluoresceinamine (Figure 6). In fact, the particle size, size distribution, and stimuli sensitivity of the labeled particles did not differ from the unmodified ones (data not shown), suggesting their similarity.

A 3-D reconstruction of such a membrane is shown in Figure 7a−c, where part a shows a distribution of the nanoparticles within the composite membrane, part b illustrates the laser-backscattering properties of the composite membrane, and part c is the superimposition of parts a and b. A fluorescent image of a sliced area at the midpoint depth of the membrane is presented in Figure 8.

The confocal images clearly reveal that the particles are dispersed throughout the whole membrane. However, instead of being single particles, they aggregate into clusters of different sizes as also observed in the SEM study, perhaps due to the difference in hydrophobicity between ethylcellulose and the particles. The clusters are connected to one another, resulting in water-rich channels. These channels serve as a primary route for solute diffusion because the

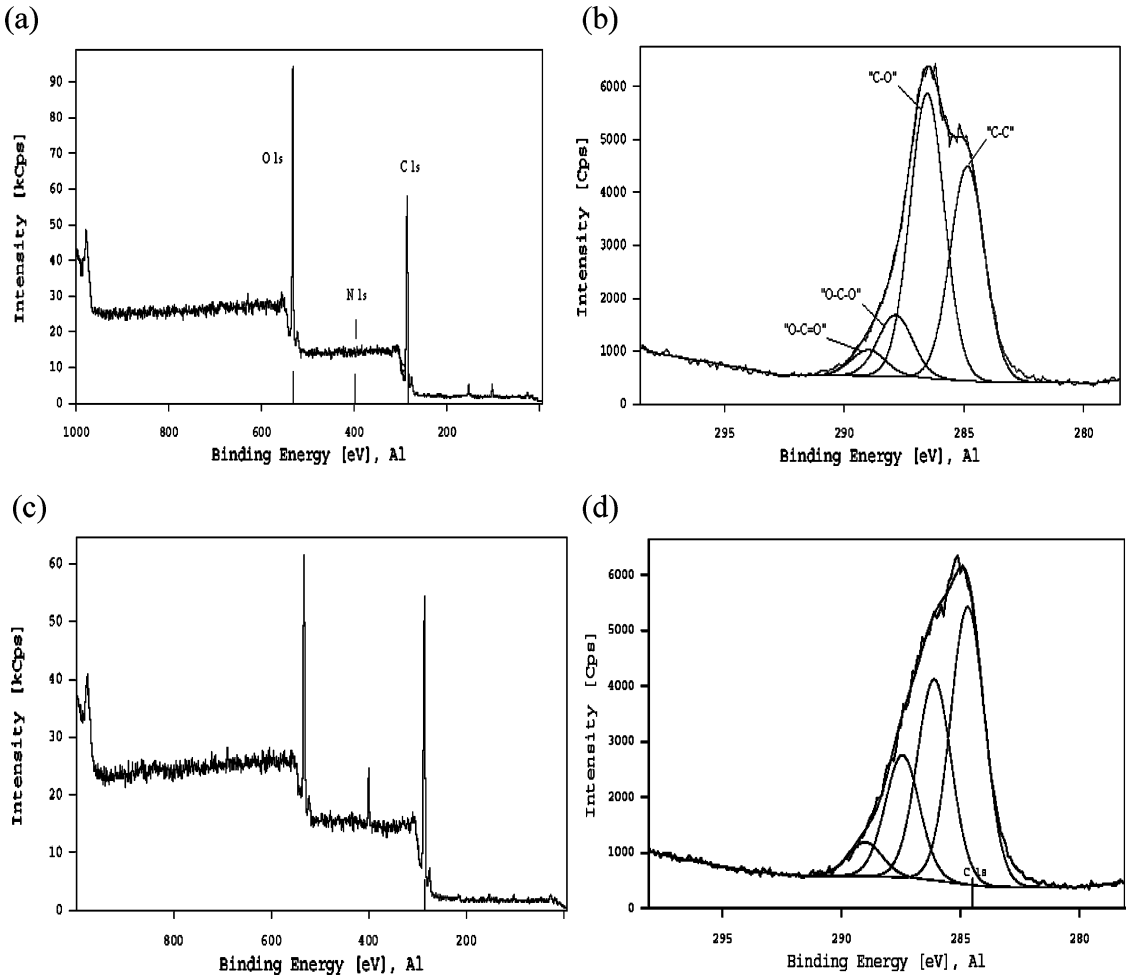

Figure 10. Survey and C1s XPS spectra of a membrane with 0% of nanoparticles (a) and (b) and with 35 wt % of nanoparticles (c) and (d).

ethylcellulose membrane is so dense that it is almost impermeable to drugs.[12] This result has provided direct evidence that the composite membrane with 35 wt % of particles achieves or surpasses the percolation threshold which was proposed for drug permeation through the membranes.[14]

One may notice in Figure 7. parts a and c, that the toplayer contains more particle clusters, which is consistent with the SEM picture, and the surface close to the laser light source appears much denser than the other surface (Figure 7b). Laser backscattering is only observed at the membrane-aqueous interface since the nanoparticles are distributed in a more homogeneous manner at the interface than the interior from where scattered light could not be detected as readily. This phenomenon is due to the loss in the intensity of the backscattered light reflected from the top surface, which is further away from the detector, as the backscattering light travels through the composite membrane.

5. Surface Chemical Composition of the Membranes. The surface chemical composition of membranes with varied concentrations (i.e., 0, 19, 30, 40, and 50 wt %) of 1:1 nanoparticles and a membrane with 35 wt % of 1:1 nanoparticles and surface coating was analyzed using XPS. The chemical structures of the nanoparticle and ethylcellulose are depicted in Figure 9. The relative element concentrations of membranes with 0, 19, and 35 wt % nanoparticles and their composition of C1s envelope are summarized in Tables

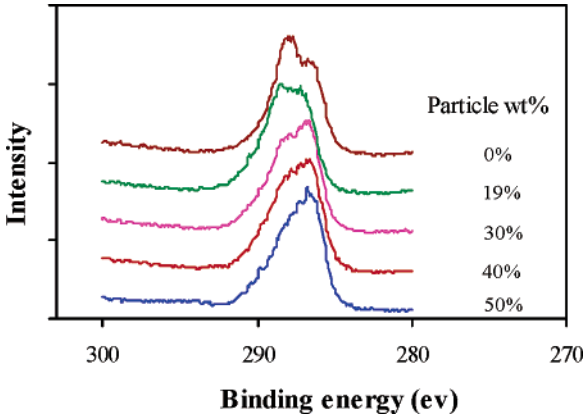

Figure 11. High-resolution C1s peak for membranes with various 1:1 nanoparticle concentration (0, 19, 30, 40, and 50 wt %).

1 and 2, respectively. Figure 10 shows survey and high-resolution C1s spectra of membranes with 0 or 35 wt % of 1:1 nanoparticles, and Figure 11 compares the C1s spectra of membranes with 0, 19, 30, 40, or 50 wt % of nanoparticles.

It is seen from these data that, with increasing nanoparticle concentration in a membrane, the N content increases, which is present in the naoparticles but absent in ethylcellulose. Though the total oxygen content and C−O carbon content decreases, C−C/C−H, O−C−O, and O−C═O carbon concentrations increase with increasing particle content. These results indicate that the concentration of the particles

on the surface increases with increasing concentration of the particles in the membrane and explain why the surface hydrophilicity, as determined by contact angle measurement,[14] of particle-containing membranes is higher than that of the ethylcellulose membrane.

It should be mentioned that assignments of the peaks of C1s in Figure 10 were a little bit arbitrary since it is difficult to separate C−N bonding from C−O bonding. Therefore, in Table 2, C−O and C−N are grouped together. However, as theoretically ethylcellulose has no nitrogen element, it is reasonable to use total N content as a measure of particle content. Besides, a peak at 289.5 ev for O−C═O environment is observed in the spectrum of ethylcellulose membrane, which is unexpected for ethylcellulose based on the chemical structure. Suspecting that this was caused by impurity, we washed the membrane and degassed extensively but could not get rid of it. After having examined the raw ethylcellulose powder and obtained the same result, we believe that this peak comes from the raw material.

The tri-layerpair coating of the polyeletrolytes did not alter noticeably the surface chemical composition. The relative amounts of elements, C, N, and O, for the coated membrane were comparable to those for the uncoated membrane and so were the results for high resolution C1s scan (data not shown). Only a trace amount, ∼ 0.1%, of Cl was detected on the surface of the coated membrane, indicating the existence of PAH. The weak XPS signals of coating may be attributable to several possibilities: (1) the coating is too thin to be differentiated by XPS that has a penetration distance ∼10 nm and (2) the chemical composition of the PAH/PAA coating is similar to that of the membrane. Good XPS signals were reported for polyethylenimine coating on a stainless steel surface[21] and for a PAH and poly(sodium styrenesulfonate) coating on poly(ethylene terephthalate) (PET).[22] In the former case, the coating is much thicker compared to three layerpairs in the present study, and the chemical compositions of the coating and the substrate differ completely. In the latter case, though the coating is also thin, the absence of nitrogen in the substrate makes the presence of PAH distinguishable. By contrast, in the present work, the nitrogen in PAH and O−C═O in PAA are all present in the composite membrane, which hinders the differentiation of the coating from the membrane by XPS.

We attempted to measure the coating thickness using an ellipsometer. However, no accurate data could be determined because the surface of the composite membrane is not smooth owing to protruding nanoparticles on the membrane surface as illustrated by the AFM images. Although the thickness of the coating cannot be quantified, qualitative indication of coating is given by AFM imaging. Besides, the presence and the effect of the coating on preventing the nanoparticle loss from the membrane surface is evidenced by AFM imaging (Figure 5).

Conclusions

The nanostructure of the composite membranes made of poly(NIPAAm-*co*-MAA) nanoparticles dispersed in a polymer matrix was characterized with SEM, XPS, AFM, and LSCM. The in situ change in particle size and porosity of the membrane immersed in buffer solutions of various pHs was visualized using AFM imaging. The particles formed clusters that in turn interconnected within the composite membranes. The size of the particles decreased while the pores increased with decreasing pH or particle dehydration. Coating the membrane with multilayers of polyelectrolytes prevented the nanoparticles from escaping from the surface of the membrane, resulting in better stability of the membrane.

Acknowledgment. This project was sponsored by the Natural Sciences and Engineering Council of Canada. Support to Kai Zhang from the University of Toronto Open Fellowship and Ben Cohen Fund is also gratefully acknowledged.

References and Notes

(1) Langer, R. *Nature* **1998**, *392*, supp. 5−10.
(2) Bae, Y. H. In *Controlled Drug Delivery Challenges and Strategies*; Park, K., Ed.; American Chemical Society: Washington, DC, 1997; pp 147−162.
(3) Qiu, Y.; Park, K. *Adv. Drug Deliv. Rev.* **2001**, *53*, 321−339.
(4) Peppas, N. A. *Curr. Opin. Colloid Interface Sci.* **1997**, *2*, 531−537.
(5) Peppas, N. A. In *Pulsatile Drug Delivery Current Application and Future Trends*; Gurny, R., Junginger, H. E., Peppas, N. A., Eds.; Wissenschaftliche Verlagsgesellschaft mbH: Stuttgart, Germany, 1993; pp 41−56.
(6) Kaneko, Y.; Sakai, K.; Okano, T. In *Biorelated Polymers and Gels Controlled Release and Biomedical Engineering*; Okano, T., Ed.; Academic Press: 1998; pp 29−70.
(7) Kost, J.; Langer, R. *Adv. Drug Deliv. Rev.* **2001**, *46*, 125−148.
(8) Kikuci, A.; Okano, T. *Adv. Drug Deliv. Rev.* **2002**, *54*, 53−77.
(9) Wu, X. Y.; Zhang, Q.; Arshady, R. In *Polymeric Biomaterials*; Arshady, R., Ed.; Citus Books: London, U.K., 2003; pp 157−194; pp 195−231.
(10) Wu, X. Y.; Yam, F. US patent 6,565,872, 2003.
(11) Yam, F.; Wu, X. Y. *Polym. Prepr.* **1999**, *40*, 312.
(12) Yam, F.; Wu, X. Y.; Zhang, Q. In *Controlled Drug Delivery: Designing Technology for the Future*; Park, K., Ed.; American Chemical Society: Washington, DC, 2000; pp 263−272.
(13) Zhang, K.; Wu, X. Y. *J. Controlled Release* **2002**, *80*, 169−178.
(14) Zhang, K.; Wu, X. Y. *Biomaterials*, in press.
(15) Huang, J.; Wu, X. Y. *J. Polym. Sci: Polym. Chem.* **1999**, *37*, 2667−2676.
(16) Wu, X. Y.; Lee, P. I. *Pharm. Res.* **1993**, *10*, 1544−1547.
(17) Moselhy, J.; Wu, X. Y.; Nicholov, R.; Kodaria, K. *J. Biomater. Sci. Polym. Ed.* **2000**, *11*(2), 123−147.
(18) Zhang, K.; Quan, C.; Huang, H.; Taulier, N.; Wu, X. Y. *J. Pharm. Pharmacol.* **2004**, in press.
(19) Horisawa, E.; Kubota, K.; Tuboi, I.; Sato, K.; Yamamoto, H.; Takeuchi, H.; Kawashima, Y. *Pharm. Res.* **2002**, *19* (2), 132−139.
(20) Chung, A. J.; Rubner, M. F. *Langmuir* **2002**, *18*, 1176−1183.
(21) Wang, T. C.; Rubner, M. F.; Cohen, R. E. *Langmuir* **2002**, *18*, 3370−3375.
(22) Tan, Q. G.; Ji, Jian; Barbosa, M. A.; Fonseca, C.; Shen, J. *Biomaterials* **2003**, *25*, 4699−4705.
(23) Chen, W.; McCarthy, T. J. *Macromolecules* **1997**, *30*, 78−86.

BM034458F